Original paper

Folia Neuropathologica

A current view of mitochondria damage and the diversity of lipopigment inclusions in neuronal ceroid lipofuscinose type 2 from rectal biopsy

Paulina Felczak[1], Aleksandra Kuźniar-Pałka[2], Agnieszka Ługowska[3], Elżbieta Stawicka[2], Sylwia Tarka[4], Hanna Mierzewska[2]

[1]Department of Neuropathology, Institute of Psychiatry and Neurology, Warsaw, Poland, [2]Clinic of Child and Adolescent Neurology, Institute of Mother and Child, Warsaw, Poland, [3]Department of Genetics, Institute of Psychiatry and Neurology, Warsaw, Poland, [4]Department of Forensic Medicine, Warsaw Medical University, Warsaw, Poland

Folia Neuropathol 2024; 62 (1): 21-31 *DOI: https://doi.org/10.5114/fn.2023.133795*

Abstract

Neuronal ceroid lipofuscinoses (NCLs) are a growing group of neurodegenerative storage diseases, in which specific features are sought to facilitate the creation of a universal diagnostic algorithm in the future. In our ultrastructural studies, the group of NCLs was represented by the CLN2 disease caused by a defect in the TPP1 gene encoding the enzyme tripeptidyl-peptidase 1. A 3.5-year-old girl was affected by this disease. Due to diagnostic difficulties, the spectrum of clinical, enzymatic, and genetic tests was extended to include analysis of the ultrastructure of cells from a rectal biopsy. The aim of our research was to search for pathognomonic features of CLN2 and to analyse the mitochondrial damage accompanying the disease. In the examined cells of the rectal mucosa, as expected, filamentous deposits of the curvilinear profile (CVP) type were found, which dominated quantitatively. Mixed deposits of the CVP/fingerprint profile (FPP) type were observed less frequently in the examined cells. A form of inclusions of unknown origin, not described so far in CLN2 disease, were wads of osmophilic material (WOMs). They occurred alone or co-formed mixed deposits. In addition, atypically damaged mitochondria were observed in muscularis mucosae. Their deformed cristae had contact with inclusions that looked like CVPs. Considering the confirmed role of the c subunit of the mitochondrial ATP synthase in the formation of filamentous lipopigment deposits in the group of NCLs, we suggest the possible significance of other mitochondrial proteins, such as mitochondrial contact site and cristae organizing system (MICOS), in the formation of these deposits. The presence of WOMs in the context of searching for ultrastructural pathognomonic features in CLN2 disease also requires further research.

Key words: *neuronal ceroid lipofuscinoses, CLN2 disease, mitochondria damage, curvilinear profiles, fingerprint profiles, rectal biopsy.*

Introduction

The neuronal ceroid lipofuscinoses (NCLs) are a genetically heterogeneous group of inherited and progressive neurodegenerative diseases of children and occasionally adults [19,22]. Clinically, the NCLs manifest early impairment of vision, progressive decline in cognitive and motor functions, seizures, and a shortened lifespan [23]. NCLs belong to the group of lysosomal storage disorders (LSD). These disorders exhibit a common hallmark of intracellular accumulation of autofluorescent lipoprotein aggregates (lipopigments) called

Communicating author:
Paulina Felczak, PhD, Department of Neuropathology, Institute of Psychiatry and Neurology, Warsaw, e-mail: pfelczak@ipin.edu.pl

Received: 01.06.2023, **Accepted:** 06.12.2023, **Online publication:** 01.03.2024

ceroid lipofuscin, which has a typical ultrastructural appearance under electron microscopy. The lipoprotein aggregates are observed in neurons and other cell types also outside the central nervous system [14]. For example, visceral storage of lipopigments was present in gut, liver, cardiomyocytes, skeletal muscle, and in the eccrine glands of skin [16,24,28]. By light microscopy, the NCLs lipopigments are brownish in haematoxylin-eosin-stained sections. These lipopigments stain with periodic acid-Schiff (PAS) and are bluish when stained with Luxol-fast blue (LFB). The presence of lipid in lipopigment may give a black appearance in Sudan black stain and a reddish appearance in oil red-O stain [2,12,13,30]. Morphologically, NCLs are marked by loss of nerve cells, foremost in the cerebral and cerebellar cortices and also in the retina, resulting in cerebral, cerebellar, and retinal atrophy [2,13]. Among extracerebral tissues, lymphocytes, skin, rectum, skeletal muscle, and occasionally conjunctiva are possible guiding targets for diagnostic identification of NCLs [2,30]. Mutations in distinct genes, called *CLN*s cause various subtypes of NCLs (*CLN1* to *CLN14*). Recent work suggests that mutation in TBC1 domain-containing kinase (TBCK)/*CLN15* may cause a new subtype of NCL referred to as CLN15 disease [14]. Most NCL subtypes are present mainly in the first decade of life and follow an autosomal-recessive mode of inheritance [2,4]. The diagnosis of NCL is based on mutation analysis, but CLN1 and CLN2 are also diagnosed by enzymatic analyses. Often, precise definition is confirmed by morphological findings, which are characteristic storage deposits of lipopigment found in NCLs subtypes. NCL-specific ultrastructural patterns encompass GRODs (granular osmiophilic deposits) and non-GROD patterns, such as curvilinear profiles (CVPs), rectilinear profiles (RLPs), or fingerprint profiles (FPPs) appearing separate or in combination as mixed forms, and which are observed in most NCL subtypes [2,9,30]. The CLN2 disease comes under the umbrella of the group of NCLs, and it is an autosomal recessive disorder caused by pathogenic variants in the tripeptidyl-peptidase1 (*TPP1*) gene. The *TPP1/CLN2* gene is located on the short arm of chromosome 11 (11p15), consisting of 13 exons and 12 introns. Mutations associated with CLN2 disease result in either reduced activity or inactivation of the lysosomal enzyme tripeptidyl peptidase 1 (TPP1), causing the accumulation of ceroid lipofuscin in the lysosomes, and massive glial activation and neuronal loss [4,10,21]. Ultrastructural analysis of lysosomal storage in CLN2 disease reveals typical CVPs, which are a morphological sign of this particular NCL disorder and occasionally also contain fragmentary FPPs and GRODs [17,22]. The disease starts between the age of 2 and 4 years (classic late-infantile phenotype). Early symptoms include seizures accompanied by ataxia in combination with a history of language delay, progressive cognitive and motor dysfunction, and visual impairment later in the disease course. To confirm a clinical suspicion of CLN2 disease, the diagnostic study should include enzyme assay (TPP1), molecular genetics, and morphological assessment [2,11,21]. The gold standard for laboratory diagnosis is the demonstration of deficient TPP1 enzyme activity in leukocytes, fibroblasts, or dried blood spots (DBS) and the identification of pathogenic variants in both alleles of the *TPP1/CLN2* gene [21]. Prenatal diagnosis is generally provided by enzyme assay and mutational analysis. Ultrastructural study of biological material from biopsy obtained at 12-15 weeks' gestation allows for the detection of CVP inclusions in subtrophoblastic endothelial cells of blood vessels [2]. No effective cure for NCL has yet been found. Proposed therapeutic attempts, including enzyme supplementation (enzyme replacement therapy – ERT), gene therapy, stem cell therapy, and anti-inflammatories, are mostly in the early stages of clinical development. Further clinical trials aim to make a faster diagnosis that will enable children to be treated before symptoms develop and will provide timely genetic information [17,19,21].

The aim of our study was to characterize the ultrastructure of intracellular lipopigment deposits in CLN2 disease in the cells of rectal mucosa, showing atypical mitochondria damage accompanying these deposits and indicating the importance of rectal biopsy in the diagnosis of NCLs.

Material and methods

The ultrastructural studies were performed on samples taken from a biopsy of the rectal mucosa of the 3.5-year-old girl with clinically suspected CLN2 disease. For electron microscope evaluation, small fragments of tissues were fixed in 2.5% glutaraldehyde solution in cacodylate buffer pH 7.4 and postfixed in 1% osmium tetroxide solution in the same buffer. After dehydration in a graded ethanol alcohol series and propylene oxide, specimens were embedded in Spurr resin. Semithin sections were stained with toluidine blue to choose the appropriate areas. Ultrathin sections were contrasted with uranyl acetate and lead citrate. The sections were examined and photographed with a transmission electron microscope (TEM) JEOL model 140 at the Nencki Institute of Experimental Biology PAS in Warsaw.

Clinical presentation

A girl aged 3.5 years was born as first child to non-consanguineous parents, with normal birth parameters. She was admitted to the Children's Neurological Department (Institute of Mother and Child) with suspicion of NCL

The development of the sick girl was disharmonious. From the age of 2 years her parents observed clumsiness, falls, tripping, and she had sleep disturbances. From the age of 35 months polymorphic seizures started, and a treatment with valproic acid was introduced followed by levetiracetam. EEG revealed focal temporal sharp and slow waves bilaterally with a tendency of generalization. The MRI showed no major abnormalities. Additionally, a quick dried blood spot detection CLN2 test was performed, which showed decreased TPP1 activity of 0.9 umol/l/h (cut-off value > 4.5), but molecular analysis did not confirm the disease. The next EEG, conducted at the age of 40 months, showed deterioration of notation with paroxysmal activity and significant photosensitivity. It was decided to extend the diagnostics by assessing the activity of lysosomal enzymes in peripheral blood leukocytes. The study showed residual TPP1 activity of 0.9 umol/l/h. Additionally, a biopsy of the rectal mucosa was performed to confirm the diagnosis. The CVP deposits often seen in CLN2 disease were detected by TEM in study specimens. The whole exome sequencing isolated from the patient's blood revealed a mutation c.622C>T/c.509-1G>C in the *TPP1* gene, finally confirming the disease. Reanalysis of DNA isolated from dried blood spot confirmed the result; the researcher performing the study admitted that it was human error. In the sick girl, from the age of 4 years, progressive developmental regression was revealed. The atonic, absence and myoclonic seizures occurred. A broad-based gait and ataxia with frequent falls were observed on neurological examination; deep reflexes were preserved. Also, her fine motor skills worsened. Her speech understanding worsened during one year of observation. Paling of fundus oculi bilaterally was detected. Early diagnosis of CLN2, i.e. before the development of full-blown disease, as was the case with our patient, enables quick action. It involves of the inclusion of enzyme replacement therapy (ERT) and thus stops the progression of the disease.

Results

Ultrastructural observations were made of selected groups of cells of the rectal mucosa, i.e. muscularis mucosae, connective tissue cells, nerve fibres, and small blood vessels. Abnormal mitochondria and deposits of NCL lipopigment, which differed in morphology, were found in most of the examined cells. Three types of inclusions were observed among the examined deposits: curvilinear profiles (CVP), fingerprint profiles (FPP), and inclusions resembling wads of osmophilic material (WOM). Curvilinear profiles (CVPs) were present in cells either as separate inclusions, usually surrounded by a membrane, or as mixed inclusions in various configurations with other types, for example CVPs/FPPs or CVPs/FPPs/WOMs. Regardless of the presence of mixed inclusions in the cells, WOM deposits also occurred separately.

Rectal mucosa cells

Muscularis mucosae

Numerous deposits of curvilinear profiles (CVPs) were often observed in the muscularis mucosae. Most often they were clusters of hook-shaped or semicircular osmophilic fibrils forming densities. The filamentous inclusions were mostly sheathed for membranes (Figs. 1, 2). Branching and dilated channels of the rough endoplasmic reticulum (RER) often bordered the inclusions near

Fig. 1. Inclusions of curvilinear profiles (CVPs) surrounded by membranes, bordering the dilated channels of the RER in muscularis mucosae (SMC). Nucleus (N), mitochondria (M). Orig. magn. 30,000×.

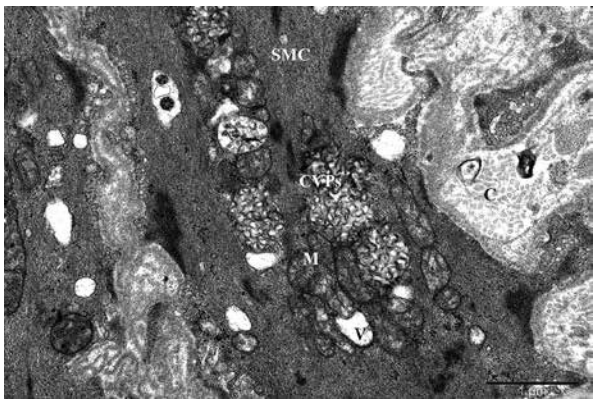

Fig. 2. Curvilinear profiles (CVPs) arranged in an alternating pattern with mitochondria (M) with partially disappeared cristae and heterogeneous matrix in muscularis mucosae (SMC). Vacuole (V), collagen (C). Orig. magn. 30,000×.

the nucleus (Fig. 1). Surrounded by CVPs deposits, there were damaged mitochondria with cristae defects and heterogeneous matrix. In addition, in the cytoplasm of muscularis mucosae, vacuolar vesicles of various sizes, bright or electron-dense, were observed (Fig. 2). Atypically deformed mitochondria associated with CVP-like filaments were found in some sectors of the muscle cell cytoplasm. The osmophilic hook-shaped filaments of these CVPs looked like they were anchored in mitochondria at sites of damaged cristae (Fig. 3). Occasionally, loosely distributed osmophilic semicircular CVP-like filaments were also found in indentations formed in residue of mitochondria (Fig. 4).

Connective tissue cells

Curvilinear profile inclusions were observed not only in muscularis mucosae, but also in mononuclear, spindle-shaped connective tissue cells, mainly in fibroblasts and fibrocytes, and in macrophage-like cells. Clusters of CVPs were visible in the cytoplasm of long fibroblast processes abundantly filled with dilated RER channels and mitochondria with heterogeneous matrix. In addition to the RER, elongated, sometimes wide channels and vesicles of the Golgi apparatus (GA) were also observed in the cytoplasm of fibroblasts (Fig. 5). Among the connective tissue cells in which CVP inclusions were observed, there were cells resembling fibrocytes in morphology. The protrusions of these cells were short, with deficient RER and GA channels and mitochondria in cytoplasm. Unlike fibroblasts, they were quite tightly enclosed by numerous collagen fibrils (Fig. 6). Elongated or rounded cells, sometimes without a visible cell nucleus, with cytoplasmic processes and vacuoles, mainly in the periphery, were also found in the connective tissue. The cytoplasm of these cells was filled with dense, osmophilic inclusions of the CVP type. The interconnected CVP inclusions

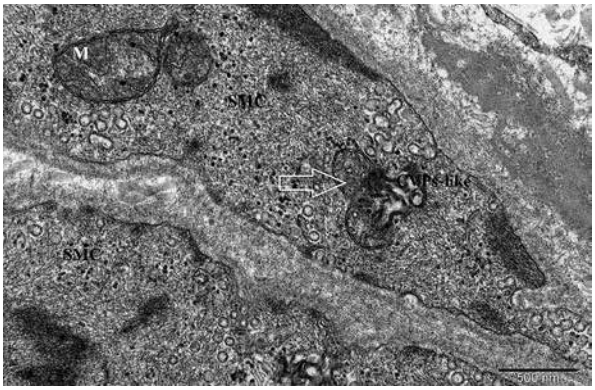

Fig. 3. Atypically deformed mitochondria (arrow) in contact with curvilinear profile (CVP)-like filaments in the muscularis mucosa (SMC). Mitochondria (M). Orig. magn. 50,000×.

Fig. 4. Vestigial mitochondria (arrow) fused with osmophilic semicircular curvilinear profile (CVP)-like filaments in muscularis mucosae (SMC). Mitochondria (M). Orig. magn. 50,000×.

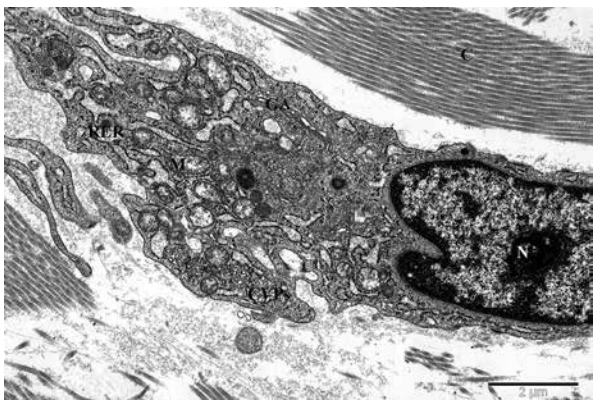

Fig. 5. Curvilinear profiles (CVPs) in contact with mitochondria (M) partially devoid of cristae and with heterogeneous matrix, and dilated RER channels in fibroblast processes. Nucleus (N), Golgi apparatus (GA), collagen (C). Orig. magn. 15,000×.

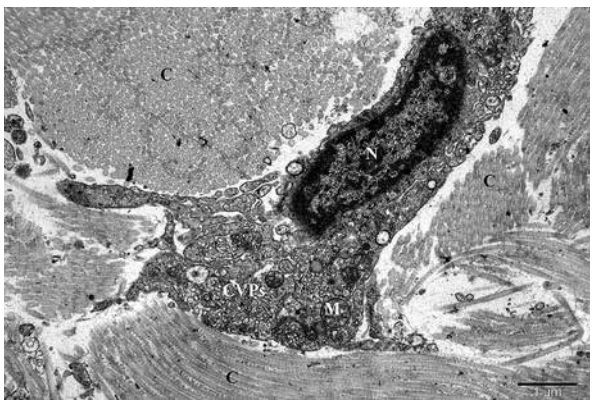

Fig. 6. Curvilinear profiles (CVPs) in the cytoplasm of fibrocyte, surrounded by densely arranged collagen fibrils (C). Nucleus (N), mitochondria (M). Orig. magn. 40,000×.

formed confluent mega inclusions with grey lipid-like structures that resembled deposits in the remodeling/degradation stage (Fig. 7).

Nerve fibres

Two types of nerve fibres in the biopsy samples, unmyelinated (Fig. 8) and myelinated (Fig. 9), were found. In unmyelinated nerve fibres, in the cytoplasm of Schwann cells with large nuclei located medially, CVPs were visible, and in their vicinity were RER channels. Axial fibres (axons) surrounded the Schwann cell and were also distributed in the concavities of the neurolemma of these cells (Fig. 8). On the other hand, in myelinated nerve fibres, osmophilic bundles were observed, which were located within the axons (Fig. 9). These inclusions were observed in peripheral locations, close to the damage axon myelin sheaths. In Figure 9, two osmophilic bundles are visible. One of them is located on the outer side of the axon in the cytoplasm of the Schwann cell and is separated from the deformed myelin sheath. The second osmophilic bundle is visible inside the myelinated axon, in the space formed by the spread myelin sheets with which it is partially continuous (Fig. 9).

Small blood vessels

Curvilinear profiles were observed in all types of small blood vessels: capillaries, venules, and arterioles. Other types of inclusions, i.e. fingerprint profiles (FPPs), were less common there and were always mixed with CVPs. Wads of osmophilic material (WOMs) have also been found occasionally. The morphology and distribution of inclusions in the cells of small vessels is shown on the examples of arterioles and venules. In arterioles, CVPs were found in both endothelial and smooth muscle cells, where they were usually located in clusters formed by several deposits (Fig. 10). In the endotheli-

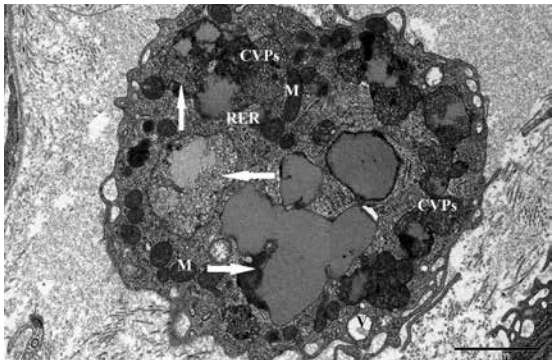

Fig. 7. Multiple curvilinear profiles (CVPs) inclusions (arrow) with visible remodeling or disintegration and lipid-load in a macrophage-like cell. Mitochondria (M), rough endoplasmic reticulum (RER), vacuole (V). Orig. magn. 15,000×.

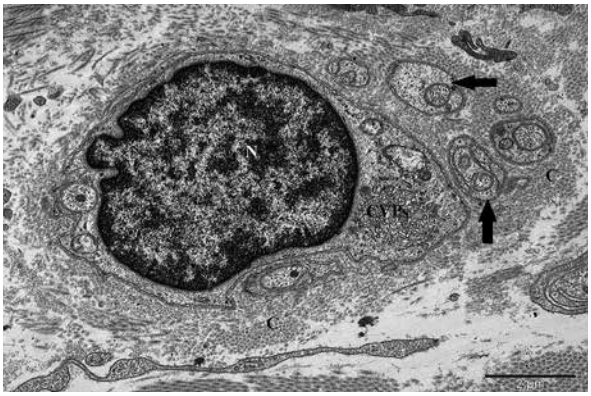

Fig. 8. Curvilinear profiles (CVPs) in the cytoplasm of a Schwann cell in an unmyelinated nerve fibre. Nucleus (N), axon (arrow), collagen (C). Orig. magn. 15,000×.

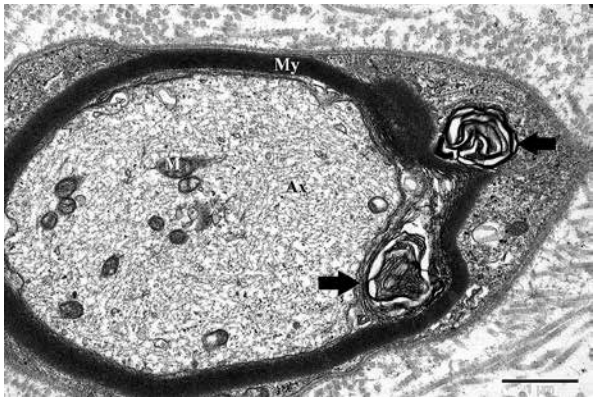

Fig. 9. Bundles of osmophilic material (arrows) near the myelin sheath (My) in a myelinated nerve fibre (Ax). Mitochondria (M). Orig. magn. 25,000×.

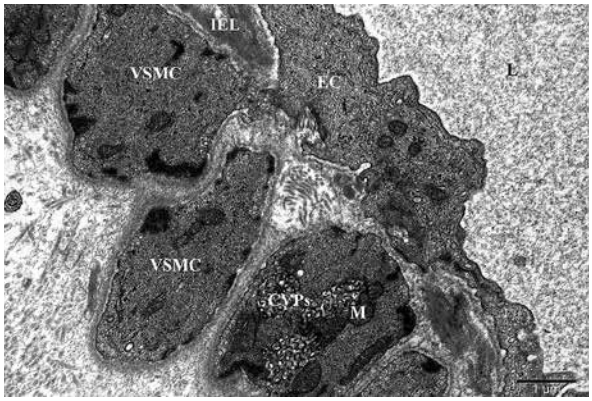

Fig. 10. Bundles of curvilinear profiles (CVPs) next to mitochondria (M) in a vascular smooth muscle cell (VSMC). Internal elastic lamina (IEL), endothelial cell (EC), lumen (L). Orig. magn. 20,000×.

um of arterioles, as well as CVPs, mixed inclusions were also observed. In this type of structure, hemispherical CVPs fibres interspersed with short, highly osmophilic fragments of FPPs predominated quantitatively. On the periphery of these mixed inclusions, variously shaped WOMs were typically found (Fig. 11). In venules, as in arterioles, inclusions were observed both in narrow smooth muscle cells and in endothelial cells (Fig. 12). The appearance of the endothelium was sometimes different from typical due to the presence of numerous protoplasmic protrusions that were located on both the luminal and abluminal sides. CVP inclusions, sometimes surrounded by membranes, were observed in the cytoplasm of these cells. In addition, ECs contained mitochondria, osmophilic Weibel-Palade bodies in transverse and longitudinal sections, and vesicles of various sizes, including pinocytic vesicles (Fig. 12). Mixed inclusions of CVPs/FPPs and differently shaped wads of osmophilic material (WOMs) adhering to them were visible in some venous endothels (Fig. 13). Sometimes mixed inclusions were a mosaic of hemispherical CVPs fibrils and highly osmophilic fingerprint profiles (FPPs) surrounded by a distinct membrane separating them from the cytoplasm (Fig. 14). Lipid droplet-like structures were found inside such inclusions. Curvilinear profiles were observed not only inside vascular cells, but also extracellularly. In the lumen of the venules,

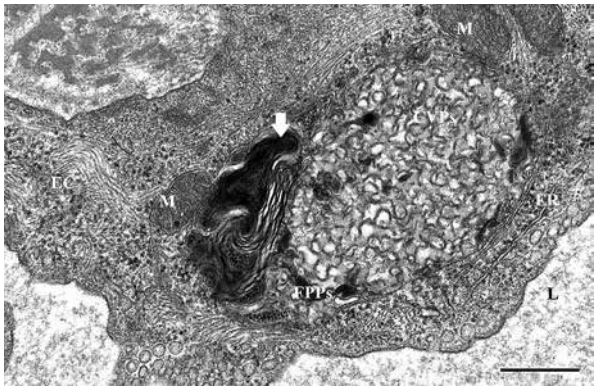

Fig. 11. Mixed inclusions formed by curvilinear profiles (CVPs) and fingerprint profiles (FPPs) and wads of osmophilic material (WOMs) (arrow) in the endothelial cell (EC) of the arteriole. Mitochondria (M), endoplasmic reticulum (ER), lumen (L). Orig. magn. 50,000×.

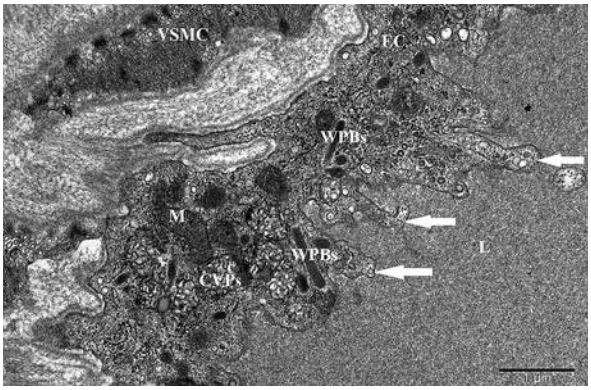

Fig. 12. Curvilinear profiles (CVPs) in the endothelial cell (EC) of the venule. Mitochondria (M), Weibel-Palade bodies (WPBs), protrusions of endothelium (arrow), vascular smooth muscle cell (VSMC), lumen (L). Orig. magn. 25,000×.

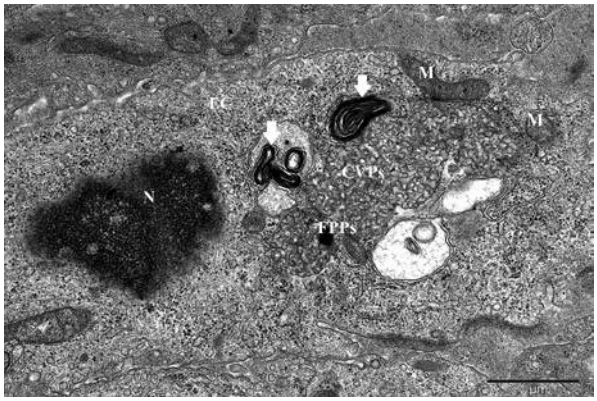

Fig. 13. Mixed inclusions formed by deposits of curvilinear profiles (CVPs), fragments of fingerprint profiles (FPPs), and wads of osmophilic material (WOMs) (arrow) in the endothelial cell (EC) of the venule. Nucleus (N), mitochondria (M). Orig. magn. 30,000×.

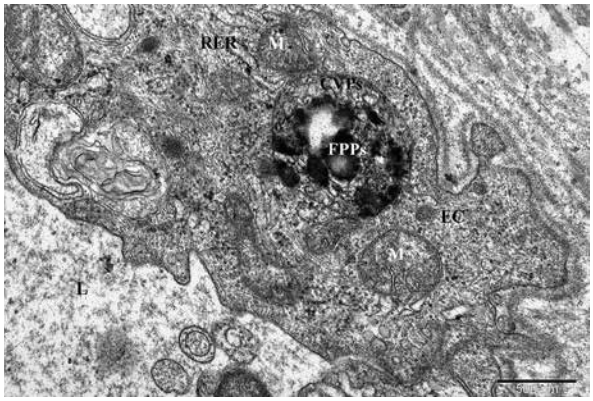

Fig. 14. Mixed inclusions formed by curvilinear profiles (CVPs) and fingerprint profiles (FPPs) surrounded by a membrane in the endothelial cell (EC) of the venule. Mitochondria (M), rough endoplasmic reticulum (RER), lumen (L). Orig. magn. 50,000×.

loosely distributed deposits of CVPs were visible in the vicinity of the ECs (Fig. 15).

Discussion

The neuronal ceroid lipofuscinoses, including the CLN2 disease we studied, may be classified according to various criteria, for example, by the age of onset of clinical signs and symptoms as well as by their underlying genetic defects, biochemical phenotype, or the ultrastructural morphology of the storage material [25]. It is difficult to indicate a universal criterion for classifying individual forms of NCL, taking into account the occurrence of mutations as a source of their variability. The growing family of NCL subtypes forces gradual changes in their ordering.

The 3.5-year-old girl described herein, suspected of having NCL, was generally within the limits of the presentation of classic (late-infantile) CLN2 disease. The presentation of the classic disease form of CLN2 is generally considered to be consistent and uniform, being well defined by age of onset (late-infantile) and multiple neurological symptoms, as well as specific electrophysiological findings and pathological changes in MRI. However, in some patients the course of the disease may differ from the typical clinical pattern, suggesting that there is a wide spectrum of CLN2 disease in terms of symptoms [17]. Interestingly, *TPP1* mutations were identified in patients with ataxia, including spinocerebellar ataxia 7 (SCAR7), which has a later onset and more restricted phenotype without epilepsy, cognitive regression, and ophthalmologic abnormalities [7]. Thus, *TPP1* mutations may be associated with late-infantile phenotype NCL (LINCL) (as in our female patient), juvenile phenotype NCL (JNCL), or spinocerebellar ataxia 7 (SCAR7) [18]. The variable phenotypes probably depend on the functional impact of TPP1 mutations, which cause complete or partial TPP1 deficiencies that were correlated with neuronal loss in cell subpopulations of the brain [7,8].

In our girl, who was suspected with clinical features of CLN2 disease, the diagnostics was extended to include molecular and enzymatic tests. Difficulties in finding pathognomonic features in CLN2 disease were the premise for extending the research with ultrastructural observations. The fact that the whole-exome sequencing (WES) in clinical conditions of inborn metabolic diseases (IMD) allows the detection of pathogenic mutations in nearly half of patients was also in favour of deeper diagnostics. Therefore, there is still a group of patients without diagnosis or requiring repeat molecular tests [37], as in the case of our girl. For ultrastructural studies, biological material from a biopsy of the rectal mucosa of female patient was used.

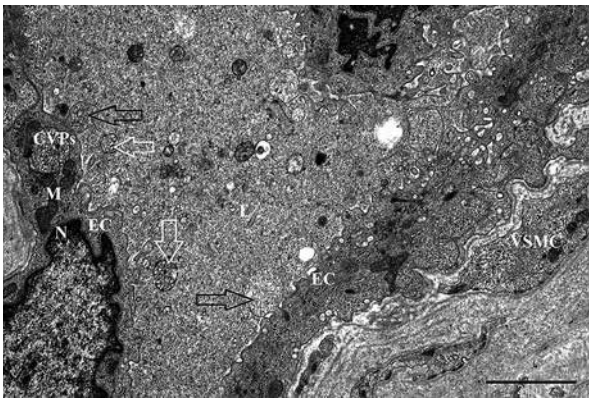

Fig. 15. Curvilinear profiles (CVPs) in the cytoplasm of endothelial cell (EC) and in the lumen (L) of the venule. Nucleus (N), mitochondria (M), protrusions of endothelium (arrow), vascular smooth muscle cell (VSMC). Orig. magn. 15,000×.

Among the most common biopsy methods of diagnosing lysosomal diseases, biopsies of the skin and conjunctiva are mentioned first, and then biopsies of skeletal muscles and peripheral nerves. From extracerebral biopsies, the rectal biopsy is one of the less frequently used [5] and still not fully appreciated diagnostic methods, despite being less invasive than, for example, skin-muscle biopsy. An important advantage of this biopsy is easy access to neuronal tissue in the myenteric ganglia. A rectal biopsy is simple to perform, scarcely traumatic, and cost-effective. As well as the epithelial and endocrine components, it includes numerous cytotypes, e.g. inflammatory cells, vascular cells, smooth muscle cells, Schwann cells, and ganglion cells, which can accumulate specific lipopigment inclusions. Diagnostic difficulties exist when the biopsy is not deep enough to allow the sampling of ganglion and smooth muscle cells [2,26]. In addition, the differentiation efficiency of lipofuscin and pathological deposits in the NCL in the case of rectal biopsy is comparable to other types of biopsy or even surpasses them [2].

The aim of our study was to analyse the ultrastructure of selected cells of the rectal mucosa in search of CVP deposits, the presence of which was expected in CLN2 disease. In a transmission electron microscope (TEM) the following were examined: smooth muscle cells, connective tissue cells (fibroblasts, fibrocytes and macrophage-like cells), and nerve fibres (myelinated and unmyelinated). Cells of small blood vessels (capillaries, venules, and arterioles) were also subjected to analysis. Accumulation of CVP deposits was observed in the examined cells, which were the quantitatively dominant type of inclusions in the CLN2 disease in our girl.

According to the literature, among the 15 different types of NCL described to date [14] CLN1 and CLN10 are marked mostly by GROD lipopigment [30]. In the CLN2 type, CVPs and sometimes fragmentary FPPs or mixed inclusions are present [2,11,25,30]. In turn, in the case of subtypes CLN3 and CLN11, most often FPPs are found [25]. The other forms of NCL generally exhibit a combination of different morphological features of inclusions, for instance, in CLN6 and CLN7 it is a mix of FPPs, RLPs, and CVPs, which can be found in neurons [25,30]. On the other hands, the majority of CLN14 disease cases occur without the storage material that is classic for NCL type [14].

In the examined cells of the rectal mucosa, CVPs inclusions were found in muscularis mucosae, in connective tissue cells, in some nerve fibres and in the cells of small blood vessels. In addition to deposits of CVPs, small FPPs inclusions have been detected mixed with CVPs, surrounded by the common membrane. These mixed inclusions were most often observed in the cytoplasm of endothelial cells and also in fibroblasts and in the nerve fibres. Ultrastructural diagnosis of CLN2 disease, as well as other types of NCL, is hampered by the lack of pathognomonic features. It is known that the presence of CVPs inclusions was most frequently found in our studies. However, treating them as an ultrastructural determinant of CLN2 disease may raise doubts because these inclusions can also be found in such types as CLN5, CLN6, CLN7, or CLN8 [25,30]. Types of NCL inclusions presented in the literature, which include CVPs, FPPs, RCLs, GRODs, and mixed inclusions [2,13,20], constitute a pool of morphological features of NCLs, which in various combinations and with varying intensity may manifest themselves in individual types of NCL. However, comprehensive studies are required to determine the specific type of NCL. Therefore, it seems very important to combine various research methods and improve NCL diagnostic algorithms that will help distinguish the types.

Certain hopes related to the search for specific features of the ultrastructure of CLN2 may be raised by the presence of unusual looking deposits detected by us in some cells from the rectal mucosa. These were WOMs that accompanied inclusions of CVPs and/or FPPs, and were also present as separate inclusions. They looked like irregularly folded accumulations of membranes. They have been observed, for example, in muscularis mucosae, in endothelial cells, and in some nerve fibres. Perhaps they represent a less common phenotype of storage deposits in CLN2 disease, but further research is required in this area.

It is known that intracytoplasmic accumulation of autofluorescent material is generally a pathogenetic hallmark of the NCL whole family, and it is ascribed to the abnormal storage of ceroid, a pathologically derived material, with similar biochemical properties to lipofuscin, the "aging pigment" [33]. The forms of NCL can be classified into 2 main categories based on the chemical identity of the predominant storage protein: those storing subunit c of the mitochondrial ATP synthase (SCMAS) and those storing sphingolipid activator proteins (SAPs) (saposins) A and D. Storage of sphingolipid activator proteins is invariably associated with GRODs, while storage of subunit c is associated with various filamentous CVP, RLP, or FPP deposits seen in TEM [2,13,20,33]. Loss of TPP1 activity leads to neuropeptide degradation failure and significant accumulation of subunit c of ATP synthase. Accumulation of subunit c has been identified not only in CLN2 disease but also in most forms of NCL, suggesting that this may not be the primary metabolic error in TPP1 deficiency [10], and confirming the non-specific nature of the described accumulations of storage material in the NCL.

If the common component of filamentous inclusions such as CVP, FPP, and RP is the subunit c of mitochondrial ATP synthase (SCMAS) [13], what biochemical components can morphologically differentiate NCL deposits? Considering the involvement of mitochondria in the pathogenesis of NCL, it should be assumed that other mitochondrial proteins, apart from SCMAS, may be involved in this process.

In the literature, in CLN2 disease, a TPP1 deficiency in fibroblasts induces a fragmentation of the mitochondrial network, probably due to a reduction in the abundance of both mitofusin 1(Mfn1) and mitofusin 2 (Mfn2), which are embedded in the outer membrane of the mitochondria [6,35].

The results of our study revealed unusual deformations of the mitochondria. It appears that the inner membranes of the mitochondria were in contact with filamentous structures that looked like CVP inclusions occupying the sites of the mitochondrial cristae.

The cristae morphology and functions are controlled by various factors, such as MICOS complex (mitochondrial contact site and cristae organizing system), the dynamin-like GTPase OPA1, the F_1 F_0 ATP synthase, and cardiolipin. Depletion of subcomplexes Mic10 or Mic60, which form MICOS complex, dramatically alter the cristae ultrastructure. In turn, loss of OPA1 oligomers, which tighten the crista junctions and maintain a negative crista junction curvature, causes mitochondrial fragmentation, and abnormal cristae architecture and dynamics. Dysfunction or loss of F_1 F_0 ATP-synthase induces concentric onion-like or balloon-like cristae morphology. Similarly, phospholipids such as cardiolipin play an essential role in shaping of the mitochondrial inner membrane [34,38]. Aberrant

cristae structures result in various neurodegenerative diseases, such as Parkinson's disease, frontotemporal dementia/Alzheimer's disease, and others [38]. As is known, NCLs are also classified as neurodegenerative disorder [20]. Moreover, there is a mutual functional interaction between the proteins shaping the architecture of the mitochondrial cristae, such as the MICOS complex, OPA1 protein, and ATP synthase [1]. It can be assumed that, apart from the confirmed presence of the subunit c of mitochondrial ATP synthase in NCL filamentous deposits, other proteins controlling the architecture of the mitochondrial cristae may co-form lipopigment deposits under pathological conditions, possibly determining the shapes of inclusions. The continuity of mitochondrial membranes with CVP-like filaments observed by us, suggesting a possible relationship between the morphology of NCL deposits and the deformations of the cristae, requires verification in the course of further research.

It is known that NCLs are characterized by the accumulation of undegraded material in lysosomes and by lysosomal dysfunction [29]. Our research showed that the observed CVP inclusions, as well as mixed CVP/FPP inclusions in CLN2 disease, were usually surrounded by a single membrane and resembled dysfunctional lysosomes loaded with heterogeneous material.

There are functional connections between mitochondria and lysosomes. Neurodegenerative diseases, such as NCLs are tightly linked to mutations in mitochondrial and lysosomal regulators. In this context, mitochondrial dysfunction leads to lysosomal impairment and build-up of autophagy by-products, whereas lysosomal imperfections trigger functional and morphological mitochondrial defects. Different pathways of communication between mitochondria and lysosomes have been described, including mitophagy, mitochondria-derived vesicles (MDVs), mitochondria-derived compartments (MDCs), and membrane contact site (MCS). The last of them, i.e. MCS, represent the known mechanism of physical interaction between mitochondria and lysosomes. This interaction allows the exchange of lipids and metabolites between these compartments [3].

This form of communication seems to be important also for the process of lipopigment accumulation in the lysosomes in CLN2 disease and perhaps for the transport of dysfunctional mitochondrial proteins, such as SCMAS, which contribute to the formation of lipopigment deposits in lysosomes.

Endolysosomal disorders are associated with the pathogenesis of virtually all lysosomal storage diseases (LSDs) including NCLs. Dysregulation of the endocytic and autophagic pathways in NCLs contributes to the accumulation of lipopigments [23]. In cells under physiological conditions, lysosomal protein TPP1 (CLN2/TPP1) with enzyme function represents a peptidase contributing to N-terminal protein degradation. Upon fusion of autophagosomes and late endosomal vesicles with lysosomal vesicles, lysosomal enzymes including TPP1 enable digestion of macromolecules [4]. In NCLs family, impaired or missing lysosomal acid hydrolases or failure of endosome-lysosome and autophagosome-lysosome fusions may result in the accumulation of undigested cargo in the lysosome, leading to LSDs [23].

Connective tissue cells may play an important role in the accumulation of NCL lipopigment deposits, as shown by our ultrastructural studies. CVP inclusions were observed in the cytoplasm of fibroblasts and fibrocytes, but the most numerous inclusions were found in macrophage-like cells. Moreover, these deposits of CVPs were interconnected into electron-dense, multi-shaped mega inclusions. Lipid-like confluent grey structures were observed within mega inclusions.

In the connective tissue, which connects and supports all other tissues, macrophages are mobile cells originating from monocytes. They are equipped with phagocytic properties and contain abundant lysosomes and phagosomes [27].

In the analysed macrophage-like cells in TEM, the occurrence of the above-mentioned confluent grey lipid-like deposits may indicate not only the abundant accumulation of the NCL lipopigment in these cells, but also its remodeling/rearrangement. Moreover, such confluent mega inclusions have not been found in other types of rectal mucosa cells.

For comparison, in another lysosomal disorder, Farber's disease, where ceramide accumulates in lysosomes, macrophages contain numerous, large, irregularly shaped inclusions with ceramide so-called Farber bodies, which are bound by lysosomal membranes [27]. Our research revealed that it is difficult to indicate the relationship between the amount of lipopigment in the examined cells from the rectal biopsy and the severity of clinical symptoms in the analysed type of CLN2. During the course of the disease, the mechanisms of remodeling and degradation of NCL deposits accumulated in lysosomes are probably activated in cells. If we assume that the studied macrophage-like cells may be involved in the process of lipopigment removal, the justification of the correlation becomes problematic. At the ultrastructural level, the essence of CLN2 disease progression seems to be a disturbed balance between the intensity of lipopigment degradation processes and the intensity of its accumulation in cells.

During our research we found the presence of lipopigment deposits in small blood vessels in CLN2 disease. Lipopigment deposits were present both in endothelium (ECs) and pericytes (PCs) of capillaries,

as well as in smooth muscle cells (VSMCs) and in ECs of arterioles and venules. These were most often CVPs and mixed deposits. For example, CVPs were observed in the EC of the arteriole, accompanied by fragmentary FPPs and WOMs. In turn, in ECs of veins, CVPs were found in the company of WOMs. According to the literature, in CLN2 disease, CVP profiles were observed in ECs [2] and in dermal VSMCs [2,36]. A similar localization of deposits concerned CLN1 disease, where granular lipopigment was subject to storage [12,36]. In turn, in the case of CLN3 and CLN6 diseases, lipopigment, i.e. CVPs, FPPs, and RLPs, were found in both ECs and VSMCs in skin biopsies, and in CLN3 disease also in rectal biopsies [12].

Own research and literature data indicate that various lipopigment inclusions are found in various cells of small vessels, i.e. ECs, PCs, and VSMCs, regardless of the type of NCLs, which may suggest the lack of tissue specificity of the deposits and the resulting diagnostic difficulties.

We also found CVP inclusions together with various cellular organelles, e.g. mitochondria, in the lumen of small vessels. This location of deposits may result from damage/rupture of vascular cells the contents of which have penetrated into the vessel.

Among the NCL deposits described in the literature, i.e. granular (GRODs) and filamentous (RLPs, FPPs, and CVPs), the latter, i.e. CVPs, are the smallest of them all. They reach a thickness of 1.9-2.4 nm [12,30]. Their delicate structure can be important in the context of movement. For comparison, the size of mitochondria ranges from 0.5 µm to approximately 3 µm, depending on the type of cell [32], which means that they are larger than the fibrils of CVPs.

The NCL diagnostic algorithms developed so far include, among others: the age of onset of the first clinical symptoms of the disease, the level of activity of specific groups of enzymes and the analysis of mutations in genes involved in the specific NCL subtype [15,30,31]. However, the difficulties associated with detecting different types of NCL, such as the CLN2 disease we studied, are due to the lack of knowledge about the specificity of these storage diseases. Such limitations encourage the expansion of the spectrum of clinical, genetic, and enzymatic tests to include ultrastructural diagnostics of biological material from biopsies. If an ambiguous result is obtained, TEM examination may determine the diagnosis of the disease.

Conclusions

Rectal biopsy is a useful method of obtaining cells with large morphological and functional diversity, which facilitates the analysis of different stages of the pathogenesis of CLN2.

The performed studies of cell ultrastructure from rectal biopsy aimed to determine the pathognomonic features of CLN2 disease. It was shown that:

– CVPs inclusions were present in all cell types of rectal mucosa studied. They were the dominant but non-pathognomonic type of inclusion in CLN2 disease and could determine its detection only in the case of combined use of clinical, genetic, and ultrastructural investigations. Less common, mixed deposits of CVPs/FPPs were predominantly found in the cells of small blood vessels;

– The WOMs, which occurred alone or in combination with other types of deposits, were probably the specific ultrastructural feature of CLN2 disease that require confirmation in the course of further research;

– The observed continuity of mitochondrial cristae with CVP-like filaments in muscularis mucosae may indicate the participation of mitochondria in the process of their remodeling;

– The found macrophage-like cells loaded with mega inclusions of NCL lipopigment may make it difficult to determine the correlation between the severity of clinical symptoms and the amount of accumulated lipopigment, assuming that mega inclusions undergo rearrangement/degradation.

Disclosure

The authors report no conflict of interest.

References

1. Anand R, Andreas S, Reichert AS, Kondadi AK. Emerging roles of the MICOS complex in cristae dynamics and biogenesis. Biology 2021; 10: 1-17.
2. Anderson GW, Goebel HH, Simonati A. Human pathology in NCL. Biochim Biophys Acta 2013; 1832: 1807-1826.
3. Audano M, Schneider A, Mitro N. Mitochondria, lysosomes, and dysfunction: Their meaning in neurodegeneration. J Neurochem 2018; 147: 291-309.
4. Baranzehi T, Kordi-Tamandani DM, Najafi M, Khajeh A, Schmidts M. Identification of a TPP1 Q278X mutation in an Iranian patient with neuronal ceroid lipofuscinosis 2: Literature review and mutations update. J Clin Med 2022; 11: 1-12.
5. Ceuterick-de Groote Ch, Martin JJ. Extracerebral biopsy in lysosomal and peroxisomal disorders. Ultrastructural findings. Brain Pathol 1998; 8: 121-132.
6. Chan DC. Mitochondria: dynamic organelles in disease, aging, and development. Cell 2006; 125: 1241-1252.
7. Chen ZR, Liu DT, Meng H, Liu L, Bian WJ, Liu XR, Zhu WW, Hea Y, Wanga J, Tanga B, Sua T, Yi YH. Homozygous missense TPP1 mutation associated with mild late infantile neuronal ceroid lipofuscinoses and the genotype-phenotype correlation. Eur J Epilepsy 2019; 69: 180-185.
8. Di Giacopo R, Cianetti L, Caputo V, La Torraca I, Piemonte F, Ciolfi A, Petrucci S, Carta C, Mariotti P, Leuzzi V, Valente EM, D'Amico A, Bentivoglio A, Bertini E, Tartaglia M, Zampino G. Protracted late infantile ceroid lipofuscinosis due to TPP1 mutations: Clin-

ical, molecular and biochemical characterization in three sibs. J Neurol Sci 2015; 356: 65-71.
9. Doccini S, Morani F, Nesti C, Pezzini F, Calza G, Soliymani R, Signore G, Rocchiccioli S, Kanninen KM, Huuskonen MT, Baumann MH, Simonati A, Lalowski MM, Santorelli FM. Proteomic and functional analyses in disease models reveal CLN5 protein involvement in mitochondrial dysfunction. Cell Death Discov 2020; 6: 1-14.
10. Gardner E, Bailey M, Schulz A, Aristorena M, Miller N, Mole SE. Mutation update: Review of TPP1 gene variants associated with neuronal ceroid lipofuscinosis CLN2 disease. Hum Mutat 2019; 40: 1924-1938.
11. Goebel HH, Wisniewski KE. Current state of clinical and morphological features in human NCL. Brain Pathol 2004; 14: 61-69.
12. Haltia M. The neuronal ceroid-lipofuscinoses. J Neuropathol Exp Neurol 2003; 62: 1-13.
13. Haltia M. The neuronal ceroid-lipofuscinoses: From past to present. Biochim Biophys Acta 2006; 1762: 850-856.
14. Kim WD, Wilson-Smillie MLDM, Thanabalasingam A, Lefrancois S, Cotman SL, Huber RJ. Autophagy in the neuronal ceroid lipofuscinoses (Batten Disease). Front Cell Dev Biol 2022; 10: 1-28.
15. Kohan R, Cismondi IA, Oller-Ramirez AM, Guelbert N, Tapia Anzolini V, Alonso G, Mole SE, de Kremer RD, de Halac IN. Therapeutic approaches to the challenge of neuronal ceroid lipofuscinoses. Curr Pharm Biotechnol 2011; 12: 867-883.
16. Lewandowska E, Lipczyńska-Łojkowska W, Modzelewska J, Wierzba-Bobrowicz T, Mierzewska H, Szpak GM, Pasennik E, Jachińska K. Kufs' disease: Diagnostic difficulties in the examination of extracerebral biopsies. Folia Neuropathol 2009; 47: 259-267.
17. Lourenco ChM, Pessoa A, Mendes CC, Rivera-Nieto C, Vergara D, Troncoso M, Gardner E, Mallorens F, Tavera L, Lizcano LA, Atanacio N, Guelbert N, Specola N, Mancilla N, de Souza CFM, Mole SE. Revealing the clinical phenotype of atypical neuronal ceroid lipofuscinosis type 2 disease: Insights from the largest cohort in the world. J Pediatr Child Health 2021; 57: 519-525.
18. Ługowska A, Purzycka-Olewiecka JK, Płoski R, Truszkowska G, Pronicki M, Felczak P, Śpiewak M, Podlecka-Piętowska A, Sitek M, Bilińska ZT, Leszek P, Bednarska-Makaruk M. Tripeptidyl peptidase 1 (TPP1) deficiency in a 36-year-old patient with cerebellar extrapyramidal syndrome and dilated cardiomyopathy. Life 2022; 12: 1-15.
19. Mole SE, Anderson G, Band HA, Berkovic SF, Cooper JD, kleine Holthaus S-M, McKay TR, Medina DL, Rahim AA, Schulz A, Smith AJ. Clinical challenges and future therapeutic approaches for neuronal ceroid lipofuscinosis. Lancet Neurol 2018; 18: 107-116.
20. Mole SE, Mitchison HM, Munroe PB. Molecular basis of the neuronal ceroid lipofuscinoses: mutations in CLN1, CLN2, CLN3, and CLN5. Hum Mutat 1999; 14: 199-215.
21. Mole SE, Schulz A, Badoe E, Berkovic SF, de Los Reyes EC, Dulz S, Gissen P, Guelbert N, Lourenco CM, Mason HL, Mink JW, Murphy N, Nickel M, Olaya JE, Scarpa M, Ingrid E. Scheffer IE, Simonati A, Specchio N, Von Löbbecke I, Wang RY, Williams RE. Guidelines on the diagnosis, clinical assessments, treatment and management for CLN2 disease patients. Orphanet J Rare Dis 2021; 16: 1-19.
22. Mole SE, Williams RE, Goebel HH. Correlations between genotype, ultrastructural morphology and clinical phenotype in the neuronal ceroid lipofuscinoses. Neurogenetics 2005; 6: 107-126.
23. Mukherjee AB, Appu AP, Sadhukhan T, Casey S, Mondal A, Zhang Z, Bagh MB. Emerging new roles of the lysosome and neuronal ceroid lipofuscinoses. Mol Neurodegener 2019; 14: 1-23.
24. Nijssen PCG, Ceuterick C, van Diggelen OP, Elleder M, Martin JJ, Teepen JLJM, Tyynelä J, Roos RAC. Autosomal dominant adult neuronal ceroid lipofuscinoses: A novel form of NCL with granular osmiophilic deposits without palmitoyl protein thioesterase 1 deficiency. Brain Pathol 2003; 13: 574-581.
25. Nita DA, Mole SE, Minassian BA. Neuronal ceroid lipofuscinoses. Epileptic Disord 2016; 18 Suppl. 2: S73-S88.
26. Pasquinelli G, Cenacchi G, Le Piane E, Russo C, Aguglia U. The Problematic issue of Kufs disease diagnosis as performed on rectal biopsies: A case report. Ultrastruct Pathol 2004; 28: 43-48.
27. Pavelka M, Roth J. Fabry disease In: Functional ultrastructure. Atlas of tissue biology and pathology. 3rd ed. Springer Wien, New York 2015; 138-139.
28. Pietrzak A, Badura-Stronka M, Kangas-Kontio T, Felczak P, Kozubski W, Latos-Bielenska A, Wierzba-Bobrowicz T, Florczak-Wyspianska J. Clinical and ultrastructural findings in an ataxic variant of Kufor-Rakeb syndrome. Folia Neuropathol 2019; 57: 285-294.
29. Plotegher N, Duchen MR. Mitochondrial dysfunction and neurodegeneration in lysosomal storage disorders. Trends Mol Med 2017; 23: 116-134.
30. Rakheja D, Bennett MJ. Neuronal ceroid-lipofuscinoses. Trans Sci Rare Dis 2018; 3: 83-95.
31. Schulz A, Kohlschütter A, Mink J, Simonati A, Williams R. NCL diseases – clinical perspectives. Biochim Biophys Acta 2013; 1832: 1801-1806.
32. Shami GJ, Cheng D, Verhaegh P, Koek G, Wisse E, Braet F. Three-dimensional ultrastructure of giant mitochondria in human non-alcoholic fatty liver disease. Sci Rep 2021; 11: 1-14.
33. Simonati A, Williams RE. Neuronal ceroid lipofuscinosis: The multifaceted approach to the clinical issues, an overview. Front Neurol 2022; 13: 1-19.
34. Stephan T, Brüser C, Deckers M, Steyer AM, Balzarotti F, Barbot M, Behr TS, Heim G, Hübner W, Ilgen P, Lange F, Pacheu-Grau D, Pape JK, Stoldt S, Huser T, Hell SW, Möbius W, Rehling P, Riedel D, Jakobs S. MICOS assembly controls mitochondrial inner membrane remodeling and crista junction redistribution to mediate cristae formation. EMBO J 2020; 39: 1-24.
35. van Beersel G, Tihon E, Demine S, Hamer I, Jadot M, Arnould T. Different molecular mechanisms involved in spontaneous and oxidative stress-induced mitochondrial fragmentation in tripeptidyl peptidase-1 (TPP-1)-deficient fibroblasts. Biosci Rep 2013; 33: 243-258.
36. Williams RE, Aberg L, Autti T, Goebel HH, Kohlschütter A, Lönnqvist T. Diagnosis of the neuronal ceroid lipofuscinoses: An update. Biochim Biophys Acta 2006; 1762: 865-872.
37. Wortmann SB, Oud MM, Alders M, Coene KLM, van der Crabben SN, Feichtinger RG, Garanto A, Hoischen A, Mirjam Langeveld M, Lefeber D, Mayr JA, Ockeloen CW, Prokisch H, Rodenburg R, Waterham HR, Wevers RA, van de Warrenburg BPC, Willemsen MAAP, Wolf NI, Vissers LELM, van Karnebeek CDM. How to proceed after "negative" exome: A review on genetic diagnostics, limitations, challenges, and emerging new multiomics techniques. J Inherit Metab Dis 2022; 45: 663-681.
38. Yang Z, Wang L, Yang Ch, Pu S, Guo Z, Wu Q, Zhou Z, Zhao H. Mitochondrial membrane remodeling. Front Bioeng Biotechnol 2022; 9: 1-18.